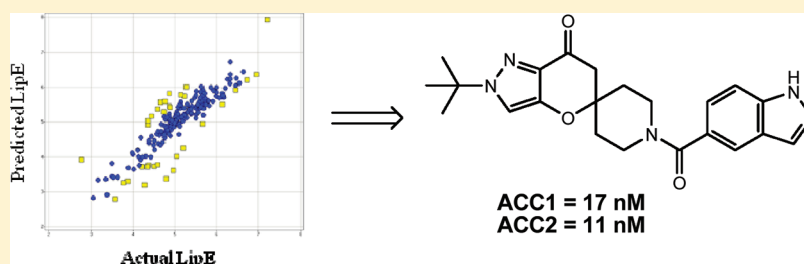


## Maximizing Lipophilic Efficiency: The Use of Free-Wilson Analysis in the Design of Inhibitors of Acetyl-CoA Carboxylase

Kevin D. Freeman-Cook,<sup>\*,†</sup> Paul Amor, Scott Bader, Leanne M. Buzon, Steven B. Coffey, Jeffrey W. Corbett, Kenneth J. Dirico, Shawn D. Doran, Richard L. Elliott, William Esler, Angel Guzman-Perez, Kevin E. Henegar, Janet A. Houser, Christopher S. Jones, Chris Limberakis, Katherine Loomis, Kirk McPherson, Sharad Murdande, Kendra L. Nelson, Dennis Phillion, Betsy S. Pierce, Wei Song, Eliot Sugarman, Susan Tapley, Meihua Tu, and Zhengrong Zhao

Pfizer Worldwide Research and Development, Eastern Point Road, Groton, Connecticut 06340, United States

**S** Supporting Information

**ABSTRACT:** This paper describes the design and synthesis of a novel series of dual inhibitors of acetyl-CoA carboxylase 1 and 2 (ACC1 and ACC2). Key findings include the discovery of an initial lead that was modestly potent and subsequent medicinal chemistry optimization with a focus on lipophilic efficiency (LipE) to balance overall druglike properties. Free-Wilson methodology provided a clear breakdown of the contributions of specific structural elements to the overall LipE, a rationale for prioritization of virtual compounds for synthesis, and a highly successful prediction of the LipE of the resulting analogues. Further preclinical assays, including *in vivo* malonyl-CoA reduction in both rat liver (ACC1) and rat muscle (ACC2), identified an advanced analogue that progressed to regulatory toxicity studies.

**■ INTRODUCTION**

Type 2 diabetes mellitus (T2DM) has become a major global health problem. The World Health Organization (WHO) estimates that more than 220 million people worldwide have diabetes. While often considered a disease of the industrialized world, more than 80% of deaths due to diabetes occur in low- and middle-income countries. Worse, the WHO predicts a 100% increase in diabetes mortality over the next two decades.<sup>1</sup> Approximately 85% of patients with T2DM are overweight or obese, a key factor underlying the development and maintenance of insulin resistance.<sup>2</sup> Because comorbidities from diabetes and obesity include stroke, cardiovascular disease, and some forms of cancer, the cumulative cost from these conditions is staggering.<sup>1</sup>

A clear correlation exists between abnormal fatty acid metabolism and the development of insulin resistance.<sup>3,4</sup> Patients who display insulin resistance also exhibit increased skeletal muscle malonyl coenzyme A (m-CoA), a key building block in fatty acid synthesis and a regulator of fatty acid oxidation.<sup>5</sup> The same insulin resistant patients also show marked suppression of fatty acid oxidation and elevated rates of *de novo* lipogenesis.<sup>3</sup> This has been hypothesized to contribute to the ectopic accumulation of hepatic and intramyocellular triglycerides in this patient population. Because of its central

role in m-CoA production, acetyl-CoA carboxylase (ACC) is a target of significant interest within the pharmaceutical industry.<sup>6–11</sup> Experiments with antisense oligonucleotides suggest that pharmacological inhibition of ACC may have the potential to reduce m-CoA levels, to lower ectopic lipid accumulation, and to improve glucose homeostasis.<sup>12</sup>

ACC is a biotin-dependent heterodimeric protein that uses bicarbonate ion to form an enzyme–biotin–carbonate complex in an adenosine triphosphate (ATP)-dependent reaction. It then transfers carbon dioxide to acetyl-CoA to form m-CoA.<sup>13</sup> Two isoforms of ACC are known [acetyl-CoA carboxylase 1 (ACC1) and acetyl-CoA carboxylase 2 (ACC2)], which differ somewhat in their tissue distribution. ACC1 is primarily located in liver and adipose tissue, while ACC2 is the major form found in skeletal and heart muscle. Our research program focused on ACC1/ACC2 dual inhibitors, to derive potential therapeutic benefit from reducing fatty acid (m-CoA) synthesis in the liver as well as stimulating fatty acid oxidation in both liver and muscle tissue.<sup>14</sup>

Screening of the Pfizer corporate compound collection, optimization of the resulting hit series, and structure-based drug

Received: November 7, 2011

Published: December 8, 2011

design efforts identified a spirochromanone series (**1**, Figure 1), which was recently described in the literature.<sup>15</sup> While **1** and

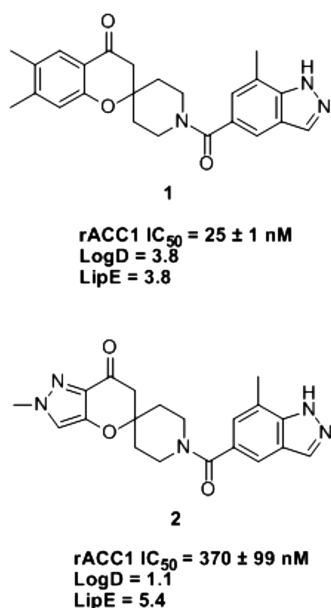


**Figure 1.** ACC1 inhibitor lead structures **1** and **2**. IC<sub>50</sub> values are the arithmetic mean of at least three independent replicates ± SEM, except where noted. Each individual IC<sub>50</sub> value is generated from single point inhibition data run in triplicate. Log *D* values are calculated using ACD laboratories Log *D* at pH = 7.4. Because of protein availability, rat ACC1 was used extensively as a surrogate for human ACC1 in screening. Ultimately, comparisons to human ACC1 were made for a subset of analogues. These showed no notable differences for all compounds tested.

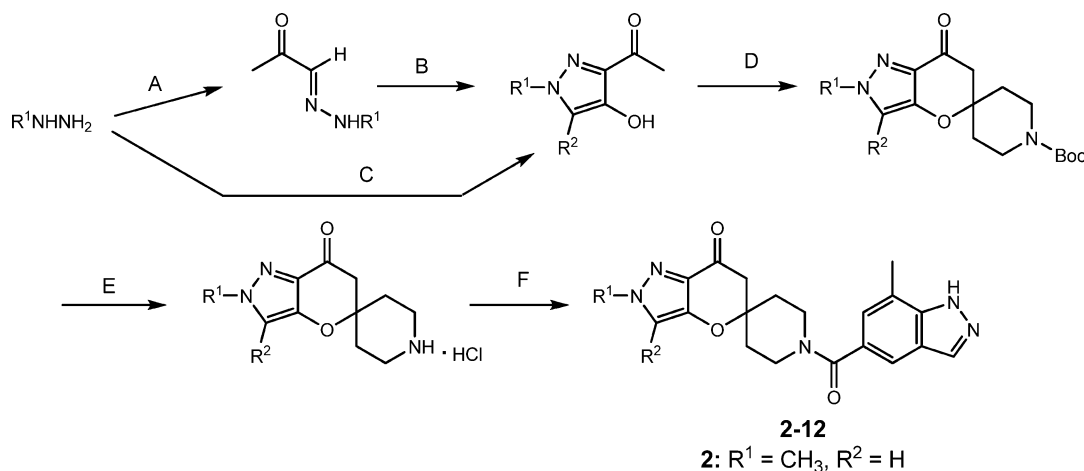
related analogues had useful potency, a major challenge in optimization of this series was a struggle with poor physicochemical properties. Lipophilic compound **1** (Log *D* = 3.8)<sup>16</sup> suffered from relatively high turnover in human liver microsomal incubations (Clint = 68 mL/min/kg)<sup>17</sup> and poor aqueous solubility (19 μM at pH = 7.4). Although the addition of lipophilicity improved potency, clearance and solubility

further deteriorated. Alternately, if polar functional groups were simply appended to the periphery of the core, different problems followed: notably compromised potency, poor permeability, and poor oral bioavailability.

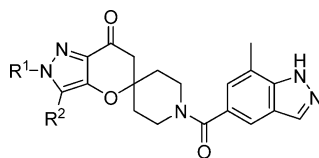
Lipophilicity is a key parameter that negatively influences metabolic stability, human ether a-go-go related gene (hERG) activity, solubility, and overall safety risk,<sup>18</sup> all of which had been concerns in the earlier spirochromanone series. In an effort to break away from the original series, several less lipophilic spiro-template structures were designed. These structures had the potential to make the same key contacts with ACC1 but contained additional polarity embedded into the core of the template. One such designed structure (**2**) proved 10-fold less potent than the more optimized spirochromanone **1**. On balance, however, when evaluating analogues in terms of their overall intrinsic potential as leads, **2** is much more efficient in terms of lipophilic ligand efficiency (LipE).<sup>19</sup> This parameter normalizes potency differences relative to a compound's lipophilicity and allows for a clear comparison between molecules. Despite its lower overall potency, **2** represents a compound with higher LipE and thus a higher intrinsic potential for further optimization to produce druglike molecules. Chemistry was therefore developed to enable the production of analogues in this chemical series (Scheme 1).

Following literature precedent, 4-hydroxy-3-acetyl pyrazoles were prepared in one or two synthetic steps in a straightforward manner.<sup>20</sup> Variation of the nitrogen substituent on the pyrazole was easily accomplished by choosing the appropriately substituted hydrazine to derivatize the 1-position. The adjacent position could be modified by choice of an appropriate 2-oxoaldehyde substrate. These 4-hydroxypyrazoles were subsequently reacted with suitably protected 4-piperidinone analogues in a base-catalyzed spiro-cyclization.<sup>15</sup> Acid-mediated deprotection, followed by coupling with 7-methyl-1*H*-indazole-5-carboxylic acid, or alternate carboxylic acid derivatives provided the final compounds for testing. Structure–activity relationship (SAR) analysis in this fused pyrazole series focused from the outset on the optimization of LipE as a means of maximizing potency at a given Log *D* and understanding the effects of making small changes to the system.

**Scheme 1.** General Synthesis of the Fused Pyrazole Core and Elaboration To Form Final Compounds<sup>a</sup>



<sup>a</sup>Conditions: (A) 2-Oxopropanal (1 equiv), AcOH, H<sub>2</sub>O, RT. (B) Glyoxal, H<sub>2</sub>O, reflux. (C) R<sup>2</sup>COCHO (6 equiv), AcOH, H<sub>2</sub>O, reflux. (D) *tert*-Butyl 4-oxopiperidine-1-carboxylate, pyrrolidine, methanol. (E) HCl, dioxane. (F) 7-Methyl-1*H*-indazole-5-carboxylic acid, TEA, HATU/EDCI or 2-chloro-4,6-dimethoxy-1,3,5-triazine, *N*-methyl morpholine. To prepare compound **2**, methylhydrazine is used in step A and glyoxal is used in step B.

Table 1. Spiropyrazole SAR<sup>a</sup>

Compound Number	R <sup>1</sup>	R <sup>2</sup>	IC <sub>50</sub> (nM)		Log <i>D</i>	LipE
			rACCl	hACC2		
1	NA	NA	25 ± 1.0	48 ± 5.7	3.8	3.8
2	Me	H	370 ± 99	650 ± 150 <sup>b</sup>	1.1	5.4
3	Me	Me	280 ± 45	470 ± 180	1.5	5.0
4	Et	H	62 ± 19	63 ± 14	1.6	5.6
5	Et	Me	28 ± 2.5	37 ± 15	2.1	5.5
6	<i>n</i> -Pr	H	48 ± 5.6	45 ± 7.0	2.1	5.2
7	<i>i</i> Pr	H	22 ± 1.7	23 ± 4.5	1.9	5.7
8	Bn	H	260 ± 56	ND	2.7	3.9
9	Cyclobutyl	H	15 ± 0.60	14 ± 2.0	2.0	5.8
10	Cyclopentyl	H	14 ± 0.60	9.4 ± 2.4	2.6	5.3
11	Cyclohexyl	H	46 ± 4.3	63 ± 15	3.1	4.2
12	<i>t</i> -Bu	H	7.0 ± 0.60	6.9 ± 0.35	2.3	5.9

<sup>a</sup>IC<sub>50</sub> values are the arithmetic mean of at least three independent replicates ± SEM, except where noted. Each individual IC<sub>50</sub> value is generated from single-point inhibition data run in triplicate. Log *D* values are calculated using ACCD labs Log *D* at pH = 7.4. LipE values are calculated using the rat ACC1 IC<sub>50</sub> value, according to the formula LipE = pIC<sub>50</sub> - Log *D*. <sup>b</sup>Arithmetic mean of two independent replicates.

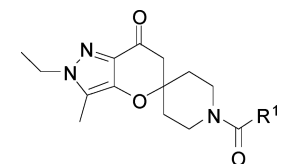
The addition of a single methyl group to **2** to produce **3** (Table 1) had a modest, beneficial effect on potency but a detrimental effect on LipE. For comparison, ethyl compound **4** provided an example of a better position to install a methyl group, exhibiting 5-fold greater potency than **3** at roughly the same Log *D*. Analogue **5** gave another example of improved LipE relative to **3**, due to its 10-fold increase in potency. This fit the original hypothesis that careful incorporation of lipophilic substituents into the proper vectors could ultimately provide the desired potency enhancement. The comparison of **6** and **7** is also intriguing. Both contain three carbon atoms appended to the pyrazole core, but a linear (*n*-propyl) arrangement as in **6** yields a less efficient analogue than the more compact (isopropyl) orientation in **7**. That trend continued in analogues such as **8**, where introduction of large, extended groups afforded inefficient analogues due to decreased potency (relative to smaller R<sup>1</sup> substituents) and increased Log *D*. Such groups were easily deprioritized for further SAR development. Cyclic substituents were tolerated at R<sup>1</sup>, as shown in compounds **9**, **10**, and **11**, but consistent with other trends, these compounds were progressively less efficient as the ring size increased. While analogues **9** and **10** have virtually identical potency, the 0.5 unit difference in log *D* is reflected in the lower LipE of **10**. The most potent and efficient pyrazole substituent was the *tert*-butyl group (compound **12**).

Because **5** demonstrated a significant potency breakthrough while maintaining a high LipE, it was chosen as a representative scaffold for SAR development in the amide “tailpiece” portion of the molecule. Synthesis of the required amine intermediate proceeded in good yields according to the general procedure shown in Scheme 1. Subsequently, custom indazole acids were coupled to this amine. A small subset of the analogues prepared is shown in Table 2.

Translation of the SAR from the earlier spirochromanone series to the new fused pyrazole series focused our efforts to optimize LipE on 5,6-fused aryl systems. Specifically, interest centered on 5-carboxy-indazole, 5-carboxy-indole, and 5-

carboxy-benzimidazole ring systems. Only modest changes in potency were observed among the many analogues examined. Methyl groups at either the 3-position of the indazole (**13**) or at the 7-position (**5**, Table 1) seemed interchangeably active and equally efficient. Installation of a methyl at both the 3- and the 7-positions gave **14**, a 12 nM compound that maintained high LipE. Extension to an ethyl substituent at either the 3-position (**15**) or the 7-position (**16**) gave analogues of lower efficiency, indicating that the ethyl groups were not optimally efficient in those vectors for ACC. The 7-ethoxy analogues (**17** and **18**) demonstrated that potency could be maintained relative to **14**. However, this came at a significant cost in lipophilicity and resulted in very poor efficiency: despite their potency, neither analogue represented an attractive avenue for further optimization. Notably, unsubstituted indazole **19** was approximately equal in LipE to both monomethyl indazole compounds (**5** and **13**) and to dimethylindazole **14**. Because **19** is 10-fold less potent than **14**, an analysis focused primarily on potency would have deprioritized the unsubstituted indazole moiety. This LipE-based analysis, on the other hand, actually highlighted the indazole moiety in **19** as an attractive option. Removal of a single nitrogen atom from the dimethylindazole system to produce dimethylindole **20** gave a familiar result: enhanced potency at the expense of efficiency. Alternatively, benzimidazoles **21** and **22** provided high LipE options, albeit at modest potency.

To more precisely define the individual contributions of various headgroups and tailpieces to the overall efficiency of the final analogues, a Free-Wilson analysis was performed (Figure 2).<sup>21</sup> Because attention had been focused on the lipophilic efficiency of the analogues throughout the early SAR analysis, the Free-Wilson methodology was utilized to assess relative contributions to LipE rather than to potency, which is most commonly used as an end point.<sup>22</sup> This allowed for a pure, direct assessment of fragment substructure LipE. Because binding of the newer pyrazole series was well aligned with the earlier spirochromanone series, examples of compounds from

Table 2. Indazole, Indole, and Benzimidazole SAR<sup>a</sup>


Compound Number	R <sup>1</sup>	rACC1 IC <sub>50</sub> (nM)	hACC2 IC <sub>50</sub> (nM)	LogD	LipE
13		29 ± 6.1	42 ± 12	2.1	5.4
14		12 ± 1.6	13 ± 2.0	2.5	5.4
15		36 ± 1.8	ND	2.6	4.9
16		31 ± 3.7	37 ± 8.0	2.6	4.9
17		11.5 ± 1.0 <sup>b</sup>	27 <sup>c</sup>	3.2	4.7
18		13 ± 1.2 <sup>b</sup>	18 <sup>c</sup>	3.7	4.2
19		100 ± 11	92 ± 17	1.6	5.4
20		9.1 ± 0.6 <sup>b</sup>	29 <sup>c</sup>	2.9	5.1
21		49 ± 3.1 <sup>b</sup>	80 ± 6.4 <sup>b</sup>	1.6	5.7
22		34 ± 1.8 <sup>b</sup>	56 ± 14 <sup>b</sup>	1.8	5.7

<sup>a</sup>IC<sub>50</sub> values are the arithmetic mean of at least three independent replicates ± SEMs, except where noted. Each individual IC<sub>50</sub> value is generated from single-point inhibition data run in triplicate. Log *D* values are calculated using ACD labs log *D* at pH = 7.4. LipE values are calculated using the rat ACC1 IC<sub>50</sub> value, according to the formula LipE = pIC<sub>50</sub> - log *D*. <sup>b</sup>Arithmetic mean of two independent replicates. <sup>c</sup>Result of a single IC<sub>50</sub> determination; the SEM in this assay is generally <20%.

both series were included in the Free-Wilson analysis. This allowed for the mathematical examination of a large number of tailpiece fragments that had only been synthesized in the spirochromanone series, enabling an evaluation of their suitability for incorporation into the fused pyrazole series. In all, 948 analogues were computationally deconstructed into their head and tail components. This provided 160 unique headgroups and 300 unique tailpieces (Figure 2). The LipE contribution of each fragment was then calculated according to the Free-Wilson methodology.

Once the headgroup and tailpiece contributions were determined, a leave-one-out (LOO) validation method was employed on three different random samples (sets 1–3) of 350 analogues from the data set (Figure 3). The *R*<sup>2</sup> values obtained for the correlation of the actual and predicted values according to this methodology were 0.87, 0.92, and 0.93. This indicated a high degree of consistent behavior and additivity within these series of ACC inhibitors. It also provided confidence in the predictive power of this method for estimating the LipE of new headgroup–tailpiece combinations.

Upon completion of this validation, focus shifted to LipE prediction for virtual analogues (i.e., novel combinations of headgroups and tailpieces) and the subsequent prioritization of a subset of those analogues for synthesis (Figure 2). The full matrix of potential combinations derived from 160 headgroups and 300 tailpieces consists of 48 000 (160 × 300) compounds. Mathematical recombination of head and tail groups allowed a prediction of LipE for each of the resulting 48 000 virtual analogues. Subsequent calculation of log *D* then allowed further prioritization. Compounds of the most interest were those predicted to have the highest LipE values, especially those with very high LipE values in the log *D* range of 1.7–2.5, which would provide the desired excellent potency in compounds with attractive physical properties. On the basis of prior SAR knowledge from both the spirochromanone and the spiro-pyrazole series, analogues in this log *D* range were the most likely to be free of complications arising from high clearance, low solubility, or low permeability.<sup>23</sup> From these considerations, a subset of 197 compounds was prioritized for synthesis, both to identify the highest quality compounds and also to test the accuracy of the Free-Wilson prediction.

Results from the 197 analogues prepared are shown in Figure 4. An arbitrary, but useful, threshold of ±0.5 LipE units was used to assess the overall accuracy of the prediction.<sup>24</sup> In all, 83% of the analogues (164/197) were found to be within ±0.5 LipE units of the Free-Wilson predicted value (blue circles, Figure 4). For 33 compounds (17%), the actual LipE values were outside of the ±0.5 unit threshold (yellow squares, Figure 4), but the majority of these (20 compounds) were still within ±0.75 units. While slightly less accurate, the predictions for these 20 analogues still resulted in measured potency values that were within 5-fold of the predicted potency values. Thus, for 184/197 analogues prepared (93%), the Free-Wilson methodology provided a LipE prediction that was quite accurate and extremely useful (within 5-fold) in the context of assessing potency and efficiency of virtual analogues. For the most part, prediction accuracy remained quite high even for the less efficient compounds (LipE < 5). This argued for a broad utility in prediction within this data set and not simply a less robust model that predicts good compounds well but struggles to handle less efficient compounds.

The data for six advanced compounds in the desired property space (log *D* = 1.7–2.5) are shown in Table 3. Not surprisingly, given the large beneficial effect on LipE observed with the *tert*-butyl group in 12 (Table 1), the *tert*-butyl moiety was present as a headgroup substituent in most of these compounds. The isopropyl group (23) and tetrahydrofuryl moiety (24) also provided very efficient analogues. The more polar headgroups of these two compounds gave products of moderate log *D* by virtue of combination with the very lipophilic dimethylindazole tailpiece. In terms of tailpieces, the majority of these six analogues contained the indazole moieties previously described, but a benzimidazole moiety was present in two compounds (25



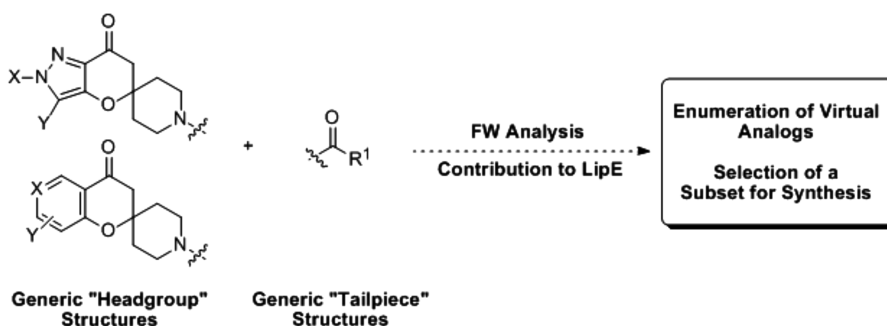


**Figure 2.** Schematic depiction of the Free-Wilson analysis for calculation of contributions to LipE from 160 headgroups and 300 tailpieces.

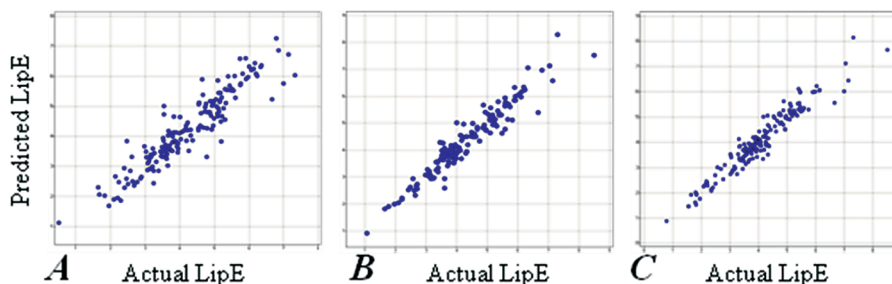


**Figure 3.** (A) LOO validation of 350 randomly sampled analogues (set 1). A total of 165 analogues predicted from this set, R-Sq value = 0.87. (B) LOO validation of 350 randomly sampled analogues (set 2). A total of 146 analogues predicted from this set, R-Sq value = 0.92. (C) LOO validation of 350 randomly sampled analogues (set 3). A total of 167 analogues predicted from this set, R-Sq value = 0.93.

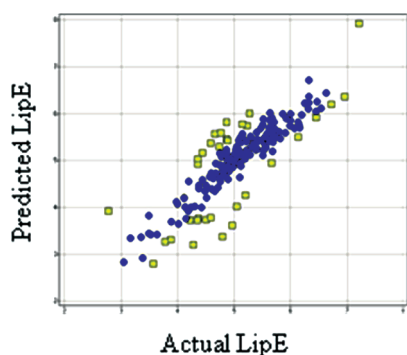


**Figure 4.** Predicted vs experimental LipE for all 197 analogues selected for synthesis. Compounds represented as blue circles (83%) are analogues where the experimental value for LipE was found to be within 0.5 units of the predicted value. Compounds represented as yellow squares (17%) are analogues where the predicted and experimental LipE values differed by more than 0.5 units.

and **26**). This group had provided efficient but less potent analogues in the earlier tailpiece SAR study (Table 2, **21** and **22**). Notably, indazole regioisomer **27** proved slightly more efficient than predicted by the Free-Wilson analysis (actual LipE = 6.0 vs predicted LipE = 5.7). More importantly, the indazole regioisomer used in **27** had been employed only sporadically prior to incorporation into analogue **27** and had never provided a compound that tested at better than 60 nM potency for ACC1. An analysis focused on potency would therefore have missed this fragment, but the Free-Wilson LipE analysis identified this indazole regioisomer tailpiece as a particularly valuable contributor to LipE. Although all compounds were relatively stable as compared to earlier lipophilic spirochromanone analogues, there seemed to be a clear advantage in microsomal stability for dimethylindazole **23** and unsubstituted indazole **28**. The polarity of **28** (relative to

both **23** and **1**) was also beneficial for aqueous solubility (300  $\mu\text{M}$  at pH = 6.5), and permeability was maintained in an RRCK cell line ( $10.9 \times 10^{-6} \text{ cm s}^{-1}$ ). Because the overall in vitro profile of **28** warranted its progression to more advanced in vivo assays, a larger scale synthesis was optimized to support these studies.

For further analysis, **28** was examined in vivo for both pharmacokinetic (PK) characteristics and efficacy in reduction of hepatic and skeletal muscle malonyl-CoA. This compound displayed a favorable rat PK profile ( $\text{Cl}_p = 26 \text{ mL/min/kg}$ ,  $V_{\text{dss}} = 2.3 \text{ L/kg}$ ,  $t_{1/2} = 4.2 \text{ h}$ ,  $F = 50\%$ , and rat plasma fraction unbound = 55%). In rat pharmacodynamic studies, **28** blocked the production of malonyl-CoA in vivo in both liver (predominantly ACC1, Figure 5A) and muscle (measured in quadriceps, predominantly ACC2, Figure 5B) after oral dosing. The apparent  $\text{ED}_{50}$  in liver was calculated to be 1.6 mg/kg. In quadriceps, the apparent  $\text{ED}_{50}$  was calculated to be 2.6 mg/kg. Maximal inhibition of malonyl-CoA synthesis occurred at the 50 mg/kg dose and reached 78 and 75% in liver and muscle, respectively.

## CONCLUSION

In summary, we have outlined an optimization that began with **2**, a weak ACC inhibitor lead, and culminated in **28**. This approach used a combination of subtle structural changes of mainly aliphatic substituents around the headgroup pyrazole ring and more substantial structural investigations around the tailpiece amide portion of the compounds. Central to this effort was a clear focus on lipophilicity and a determination to identify the modifications, which led to the most efficient (not simply the most potent) analogues. Application of Free-Wilson analysis proved useful in this respect, allowing not only a clear assessment of each group's respective contribution to LipE but also a highly accurate prospective prediction of the LipE for virtual compounds. This effort resulted in the design and

Table 3. Structure, Potency, LipE, and Microsomal Stability Data for Six Advanced Analogues<sup>a</sup>

Compound Number	R <sup>1</sup>	R <sup>2</sup>	R <sup>3</sup>	rACC1 IC <sub>50</sub> (nM)	hACC2 IC <sub>50</sub> (nM)	LogD	Predicted LipE	Actual LipE	HLM Stability Clint (mL/min/kg)
23		H		12 ± 1.1	14 ± 4.8	2.4	5.5	5.5	< 8
24		Me		21 ± 1.5	20 ± 4.5 <sup>b</sup>	1.8	5.9	5.9	23.1
25		H		9.6 ± 1.3	7.4 ± 1.9	1.8	6.0	6.2	12.4
26		H		10 ± 0.43	6.6 ± 1.6	2.0	5.9	6.0	15.1
27		H		13 ± 6.0	21 ± 5.1	1.9	5.7	6.0	13.1
28		H		17 ± 1.8	11 ± 1.1	1.8	6.0	6.0	< 8

<sup>a</sup>IC<sub>50</sub> values are the arithmetic mean of at least three independent replicates ± SEMs, except where noted. Each individual IC<sub>50</sub> value is generated from single-point inhibition data run in triplicate. Log *D* values are calculated using ACD labs log *D* at pH = 7.4. Actual LipE values are calculated using the rat ACC1 IC<sub>50</sub> value, according to the formula LipE = pIC<sub>50</sub> – log *D*. <sup>b</sup>Arithmetic mean of two independent replicates.

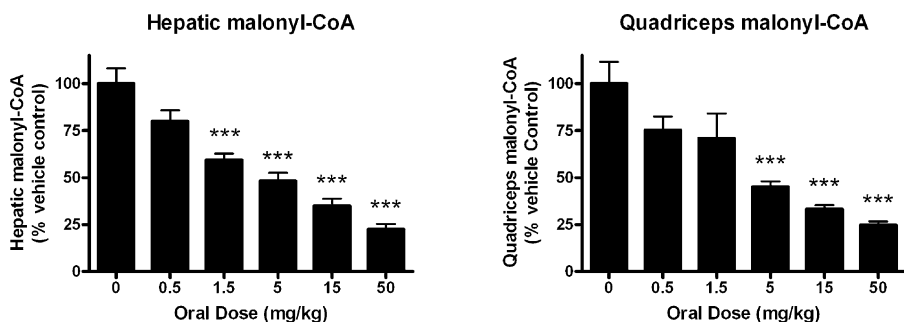


Figure 5. Bar graphs of oral dose vs hepatic malonyl Co-A levels (percent relative to control, left panel) and oral dose vs quadriceps malonyl Co-A levels (percent relative to control, right panel).

synthesis of **28**, a novel ACC1/2 inhibitor that advanced to regulatory toxicity studies as a potential treatment for diabetes.

## EXPERIMENTAL SECTION

**Materials and Methods.** Reagents and solvents were of commercial quality and were used without further purification unless otherwise noted. Proton NMR chemical shifts are given in parts per million downfield from tetramethylsilane and were recorded on a Varian Mercury Plus 300 MHz, Varian Unity 400 or 500 MHz (megaHertz) spectrometer (Varian Inc.; Palo Alto, CA). NMR chemical shifts are given in parts per million downfield from tetramethylsilane (for proton) or fluorotrichloro-methane (for fluorine). Multiplicities are given as s (singlet), bs (broad singlet), d (doublet), t (triplet), dt (double of triplets), and m (multiplet). Mass

spectra were recorded on a Waters (Waters Corp., Milford, MA) Micromass Platform II spectrometer. Unless otherwise specified, mass spectra were recorded on a Waters Micromass Platform II spectrometer. Flash chromatography was performed according to the method described by Still et al. (*J. Org. Chem.*, 1978, 43, 2923). All Biotage purifications, discussed herein, were performed using either a 40M or 40S Biotage column containing KP-SIL silica (40–63 μM, 60 Å) (Biotage AB; Uppsala, Sweden). All CombiFlash purifications, discussed herein, were performed using a CombiFlash Companion system (Teledyne Isco, Lincoln, NE) utilizing packed RediSep silica columns. All tested compounds were determined to be >95% pure by high-performance liquid chromatography (HPLC). The compounds and intermediates described below were generally named according to the IUPAC (International Union for Pure and Applied Chemistry)

recommendations on Nomenclature of Organic Chemistry and the CAS Index rules.

**HPLC Analytical Conditions.** Method LC-1: column, Waters ACQUITY Ultra Performance LC BEH C<sub>18</sub> column, 2.1 mm × 30 mm, 1.7 μm, 0.05% TFA 95/5 to 5/95 water/acetonitrile; flow rate, 1.3 mL/min; run time, 1.1 min. Method LC-2: column, Waters XTerra C<sub>18</sub> 4.6 mm × 50 mm, 3.5 μm column. Solvents A and B were Water w/0.1% TFA and acetonitrile w/0.1% TFA, respectively. Nine minute total method time with 5–95% B over 5.83 min. Mass spectral data were acquired from 180 to 850 amu in electrospray positive mode. The flow rate was 2.0 mL/min.

**Rat ACC1 Assay Description.** Rat ACC1 was purified from rat liver as previously described.<sup>14</sup> For ACC1 inhibition studies, test compounds were dissolved in dimethyl sulfoxide (DMSO), serially diluted in DMSO, and were added in replicate to 96-well plates. A comparable volume of DMSO was added to control wells. The enzyme was activated for 30 min at 37 °C in buffer containing: 50 mM HEPES (pH 7.5), 10 mM MgCl<sub>2</sub>, 10 mM tripotassium citrate, 6 mM DTT, 0.75 mg/mL BSA, and 0.8 μg/mL ACC prior to addition to assay wells. After a 10 min enzyme–compound preincubation, the reaction was initiated at room temperature in a fume hood by the addition of the substrate solution (containing 2.4 mM acetyl-CoA, 38.4 mM KHCO<sub>3</sub>, 1.6 mM <sup>14</sup>C-NaHCO<sub>3</sub>, and 8.0 mM ATP). The final assay volume of 100 μL per well consisted of 46 mM HEPES (pH 7.5), 7.5 mM MgCl<sub>2</sub>, 7.5 mM tripotassium citrate, 2.8 mM DTT, 0.5 mg/mL BSA, 2.0 mM ATP, 600 μM acetyl-CoA tritium salt, 9.6 mM potassium bicarbonate, 0.6 μg/mL ACC1, and 0.4 mM <sup>14</sup>C-NaHCO<sub>3</sub> (58 mCi/mmol). After 20 min, the reaction was terminated by the addition of 3 N hydrochloric acid (HCl) with the concomitant liberation of nonreacted NaHCO<sub>3</sub> as CO<sub>2</sub>. Plates were dried overnight at 50 °C to allow complete <sup>14</sup>C–CO<sub>2</sub> liberation. The following day, water and OptiPhase Supermix liquid scintillation fluid were added to the dried wells now containing <sup>14</sup>C-malonyl-CoA. Following vigorous shaking, the amount of <sup>14</sup>C in each assay well was quantified using Microbeta LSC luminescence counter.

**Human ACC2 Assay Description.** Human ACC2 was purified, and hACC2 inhibition assays were performed as previously described.<sup>15</sup> Briefly, ACC2 was expressed in CHO cells, and recombinant ACC2 was isolated using soft-link Avidin (Promega, Madison, WI). ACC2 inhibition assays were performed using the Transcreeper ADP detection FP assay kit (Bellbrook Laboratories, Madison, WI) using the manufacturers' conditions and read using an Envision Fluorescence reader (Perkin-Elmer) using a 620 excitation Cy5 FP general dual mirror, 620 excitation Cy5 FP filter, 688 emission (S), and a 688 (P) emission filter.

**Synthesis of 2'-(tert-Butyl)-1-(1H-indazole-5-carbonyl)-2'H-spiro[piperidine-4,5'-pyrano[3,2-c]pyrazol]-7'(6'H)-one (28).** A mixture of 1H-indazole-5-carboxylic acid (2.70 g, 16.7 mmol), 2-chloro-4,6-dimethoxy-1,3,5-triazine (2.93 g, 16.7 mmol), and N-methylmorpholine (1.72 g, 16.7 mmol) in DMF (98.1 mL) was stirred for 1 h at room temperature. 2'-(tert-Butyl)-2'H-spiro[piperidine-4,5'-pyrano[3,2-c]pyrazol]-7'(6'H)-one hydrochloride (5.0 g, 17 mmol) and an additional quantity of N-methylmorpholine (3.44 g, 33.3 mmol). The reaction mixture was then stirred at ambient temperature for 1.5 h. The mixture was filtered to remove insoluble solids. Then, aqueous ammonium chloride was added to the filtrate, and the mixture was extracted with EtOAc. The layers were separated, and the aqueous layer was extracted with EtOAc (3×). The combined organic layers were washed with water and saturated aqueous sodium chloride, dried (Na<sub>2</sub>SO<sub>4</sub>), filtered, and concentrated under reduced pressure. The crude product was purified via medium pressure chromatography (SiO<sub>2</sub>) eluting with a gradient of chloroform:methanol (100:0 to 97:3) to deliver 6.8 g (89%) of 28 as a pale yellow foam. <sup>1</sup>H NMR (500 MHz, DMSO-*d*<sub>6</sub>) δ 1.51 (s, 9 H), 1.72–1.78 (m, 2 H), 1.95 (br. s., 2 H), 2.75 (s, 2 H), 3.18 (br. s., 2 H), 4.23 (br.s., 2 H), 7.40 (dd, *J* = 8.5, 1.5 Hz, 1 H), 7.58 (d, *J* = 8.5 Hz, 1 H), 7.81 (s, 1 H), 7.86 (s, 1 H), 8.14 (s, 1 H), 13.26 (br. s., 1 H). MS (ES+) *m/z* 408 (MH<sup>+</sup>). HPLC (method LC-1) retention time = 0.38 min. An analytical sample could be obtained by dissolving the solid in dichloromethane and filtering through a plug of silica gel. The filtrate

was concentrated to afford a yellow solid, which was triturated with ether for 1 h. The solid was filtered and dried in vacuo to afford a white solid; mp 257 °C. Anal. calcd for C<sub>22</sub>H<sub>25</sub>N<sub>5</sub>O<sub>3</sub>: C, 64.85; H, 6.18; N, 17.19. Found: C, 64.59; H, 6.40; N, 16.87.

## ■ ASSOCIATED CONTENT

### 📄 Supporting Information

Experimental details for the synthesis of key intermediates as well as compounds 1–27. This material is available free of charge via the Internet at <http://pubs.acs.org>.

## ■ AUTHOR INFORMATION

### Corresponding Author

\*Tel: 858-526-4844. E-mail: [kevin.freeman-cook@pfizer.com](mailto:kevin.freeman-cook@pfizer.com).

### Present Address

<sup>†</sup>Pfizer Worldwide Research and Development, 10770 Science Center Drive, San Diego, California 92121.

## ■ ACKNOWLEDGMENTS

We thank Katherine Brighty, Martin Edwards, Robert Hoffman, and David Griffith for editorial suggestions and help with proofreading.

## ■ ABBREVIATIONS USED

WHO, World Health Organization; T2DM, type 2 diabetes mellitus; ACC1, acetyl-CoA carboxylase 1; ACC2, acetyl-CoA carboxylase 2; LipE, lipophilic ligand efficiency; m-CoA, malonyl coenzyme A; ATP, adenosine triphosphate; SEM, standard error of measurement; hERG, human ether a-go-go related gene; AcOH, acetic acid; HCl, hydrochloric acid; TEA, triethyl amine; HATU, 2-(1H-7-azabenzotriazol-1-yl)-1,1,3,3-tetramethyl uronium hexafluorophosphate methanaminium; EDCl, 1-ethyl-3-(3-dimethylaminopropyl) carbodiimide; SAR, structure–activity relationships; PK, pharmacokinetic

## ■ REFERENCES

- (1) World Health Organization fact sheets. <http://www.who.int/mediacentre/factsheets/fs312/en/index.html> (accessed July 18, 2011).
- (2) Mokdad, A. H.; Ford, E. S.; Bowman, B. A.; Dietz, W. H.; Vinicor, F.; Bales, V. S.; Marks, J. S. Prevalence of obesity, diabetes, and obesity-related health risk factors, 2001. *J. Am. Med. Assoc.* **2003**, *289* (1), 76–79.
- (3) Savage, D. B.; Petersen, K. F.; Shulman, G. I. Disordered lipid metabolism and the pathogenesis of insulin resistance. *Physiol. Rev.* **2007**, *87* (2), 507–520.
- (4) Shulman, G. I. Cellular mechanisms of insulin resistance. *J. Clin. Invest.* **2000**, *106* (2), 171–176.
- (5) Bandyopadhyay, G. K.; Yu, J. G.; Ofrecio, J.; Olefsky, J. M. Increased Malonyl-CoA levels in muscle from obese and type 2 diabetic subjects lead to decreased fatty acid oxidation and increased lipogenesis; thiazolidinedione treatment reverses these defects. *Diabetes* **2006**, *55* (8), 2277–2285.
- (6) Bourbeau, M. P.; Allen, J. G.; Gu, W. Recent advances in acetyl-CoA carboxylase inhibitors. *Annu. Rev. Med. Chem.* **2010**, *45*, 95–108.
- (7) Chonan, T.; Tanaka, H.; Yamamoto, D.; Yashiro, M.; Oi, T.; Wakasugi, D.; Ohoka-Sugita, A.; Ito, F.; Koretsune, H.; Hiratate, A. Design and synthesis of disubstituted (4-piperidinyl)-piperazine derivatives as potent acetyl-CoA carboxylase inhibitors. *Bioorg. Med. Chem. Lett.* **2010**, *20* (13), 3965–3968.
- (8) Corbett, J. W. Review of recent acetyl-CoA carboxylase inhibitor patents: mid-2007 - 2008. *Expert Opin. Ther. Pat.* **2009**, *19* (7), 943–956.
- (9) Corbett, J. W.; Harwood, J. H. Jr. Inhibitors of mammalian acetyl-CoA carboxylase. *Recent Pat. Cardiovasc. Drug Discovery* **2007**, *2* (3), 162–180.

(10) Shinde, P.; Srivastava, S. K.; Odedara, R.; Tuli, D.; Munshi, S.; Patel, J.; Zambad, S. P.; Sonawane, R.; Gupta, R. C.; Chauthaiwale, V.; Dutt, C. Synthesis of spiro[chroman-2,4'-piperidin]-4-one derivatives as acetyl-CoA carboxylase inhibitors. *Bioorg. Med. Chem. Lett.* **2009**, *19* (3), 949–953.

(11) Chonan, T.; Oi, T.; Yamamoto, D.; Yashiro, M.; Wakasugi, D.; Tanaka, H.; Ohoka-Sugita, A.; Io, F.; Koretsune, H.; Hiratate, A. 4-Piperidinyl-piperazine: A new platform for acetyl-CoA carboxylase inhibitors. *Bioorg. Med. Chem. Lett.* **2009**, *19* (23), 6645–6648.

(12) Savage, D. B.; Choi, C. S.; Samuel, V. T.; Liu, Z.-X.; Zhang, D.; Wang, A.; Zhang, X.-M.; Cline, G. W.; Yu, X. X.; Geisler, J. G.; Bhanot, S.; Monia, B. P.; Shulman, G. I. Reversal of diet-induced hepatic steatosis and hepatic insulin resistance by antisense oligonucleotide inhibitors of acetyl-CoA carboxylases 1 and 2. *J. Clin. Invest.* **2006**, *116* (3), 817–824.

(13) Polakis, S. E.; Guchhait, R. B.; Zwergel, E. S.; Lane, M. D.; Cooper, T. G. Acetyl coenzyme A carboxylase system of *Escherichia coli*. Mechanisms of the biotin carboxylase and carboxyltransferase catalyzed reactions. *J. Biol. Chem.* **1974**, *249* (20), 6657–67.

(14) Harwood, H. J. Jr.; Petras, S. F.; Shelly, L. D.; Zaccaro, L. M.; Perry, D. A.; Makowski, M. R.; Hargrove, D. M.; Martin, K. A.; Tracey, W. R.; Chapman, J. G.; Magee, W. P.; Dalvie, D. K.; Soliman, V. F.; Martin, W. H.; Mularski, C. J.; Eisenbeis, S. A. Isozyme-nonspecific N-Substituted Bipiperidylcarboxamide Acetyl-CoA Carboxylase Inhibitors Reduce Tissue Malonyl-CoA Concentrations, Inhibit Fatty Acid Synthesis, and Increase Fatty Acid Oxidation in Cultured Cells and in Experimental Animals. *J. Biol. Chem.* **2003**, *278* (39), 37099–37111.

(15) Corbett, J. W.; Freeman-Cook, K. D.; Elliott, R.; Vajdos, F.; Rajamohan, F.; Kohls, D.; Marr, E.; Zhang, H.; Tong, L.; Tu, M.; Murdande, S.; Doran, S. D.; Houser, J. A.; Song, W.; Jones, C. J.; Coffey, S. B.; Buzon, L.; Minich, M. L.; Dirico, K. J.; Tapley, S.; McPherson, R. K.; Sugarman, E.; James Harwood, H.; Esler, W. Discovery of small molecule isozyme non-specific inhibitors of mammalian acetyl-CoA carboxylase 1 and 2. *Bioorg. Med. Chem. Lett.* **2010**, *20* (7), 2383–2388.

(16) This Log *D* value (and all others in this manuscript) are calculated Log *D* values, using ACD laboratories software (at pH = 7.4).

(17) Obach, R. S. The prediction of human clearance from hepatic microsomal metabolism data. *Curr. Opin. Drug Discovery Dev.* **2001**, *4* (1), 36–44.

(18) Hughes, J. D.; Blagg, J.; Price, D. A.; Bailey, S.; DeCrescenzo, G. A.; Devraj, R. V.; Ellsworth, E.; Fobian, Y. M.; Gibbs, M. E.; Gilles, R. W.; Greene, N.; Huang, E.; Krieger-Burke, T.; Loesel, J.; Wager, T.; Whiteley, L.; Zhang, Y. Physicochemical drug properties associated with in vivo toxicological outcomes. *Bioorg. Med. Chem. Lett.* **2008**, *18* (17), 4872–4875.

(19) Edwards, M. P.; Price, D. A. Role of physicochemical properties and ligand lipophilicity efficiency in addressing drug safety risks. *Annu. Rep. Med. Chem.* **2010**, *45*, 381–391.

(20) Begtrup, M.; Nytoft, H. P. Reactions of Glyoxals with Hydrazones: A New Route to 4-Hydroxypyrazoles. *J. Chem. Soc., Perkin Trans. 1* **1985**, *1*, 81–86.

(21) Free, S. M. Jr.; Wilson, J. W. A Mathematical Contribution to Structure-Activity Studies. *J. Med. Chem.* **1964**, *7* (4), 395–399.

(22) Patel, Y.; Gillet, V. J.; Howe, T.; Pastor, J.; Oyarzabal, J.; Willett, P. Assessment of Additive/Nonadditive Effects in Structure-Activity Relationships: Implications for Iterative Drug Design. *J. Med. Chem.* **2008**, *51* (23), 7552–7562.

(23) The calculation of Log *D* also allowed a calculation of predicted potency (predicted pIC<sub>50</sub> = predicted LipE + log *D*).

(24) This level of accuracy for predicted LipE on a logarithmic scale corresponds to a 3-fold accuracy in potency prediction.